LANGMUIR

pubs.acs.org/Langmuir Article

Low Temperature NO and CO Conversion with a Mechanistic Approach on Ru-Composed Cerium Oxide

Rahul D. Kerkar* and Arun.V. Salker*

Cite This: *Langmuir* 2024, 40, 15721−15730 Read Online

ACCESS | Metrics & More | Article Recommendations | Supporting Information

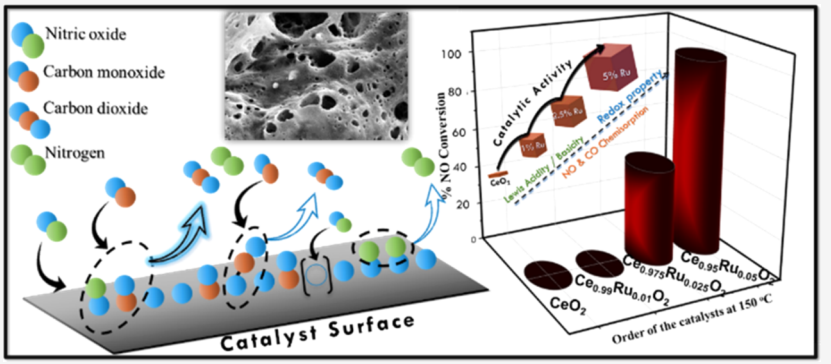

ABSTRACT: Catalytic reduction of NO with CO at a lower temperature is an extremely challenging task, thus requiring conceivable surfaces to overcome such issues. Ru-substituted CeO_2 catalysts prepared via the solution combustion method were employed in CO oxidation and NO−CO conversion studies. The characterization for material formation and surface structure was carried out through XRD, SEM, TEM, and BET surface area. The catalytic study revealed the promising behavior of 5% Ru in CeO_2 for the 100% conversion of NO−CO at 150 °C, proving it to be an excellent exhaust material. These observed results are also supported by temperature-programmed studies, i.e. TPD of NO and CO in addition to NH_3-TPD and H_2-TPR for their convincible surface interaction that is inclined toward a significant change in the conversion path. Additionally, the proposed mechanism, based on the experimental evidence, sheds light on the NO−CO redox reaction, directing the reaction pathway toward the Langmuir−Hinshelwood and Mars-Van Krevelen-type route. Moreover, the exceptional performance can be attributed to the strategic incorporation of Ru in CeO_2, where the strong interaction of Ru−Ce is able to gain a high synergy for NO and CO conversion.

Downloaded via GYEONGSANG NATL UNIV on November 11, 2024 at 07:56:01 (UTC).
See https://pubs.acs.org/sharingguidelines for options on how to legitimately share published articles.

INTRODUCTION

For the past many decades, heterogeneous catalysis has gained huge attention in many catalytic reactions, including environment-related detoxification reactions. Knowing the fact about the rise in gaseous pollutants, reducing their amount using a catalytic process is the only way to maintain the purity of atmospheric air and other environmental issues. The exhaust pollutants such as CO, NO, and HC are the major products that cause health and environmental deterioration. Thus, targeting specific gases like NO and CO or NO and HC simultaneously can significantly contribute to the elimination of such pollutants. Converting NO and CO simultaneously using various catalytic materials has been known for a long time.[1] Although this idea is quite interesting, the development of a catalyst for converting NO to N_2 and CO to CO_2 at a lower temperature is a challenging task as NO is quite stable at a higher temperature.

Most of the catalysts that have been reported for such NO−CO conversion are based on transition metal oxide series (such as Cu−O, Mn−O, Co−O, Fe−O, etc.),[2−7] as their unique oxidation-switching property makes them superior catalytic materials. In the domain of material design, bimetallic compositions also offer the potential for achieving exceptional catalytic performance.[8] In addition to these oxide catalysts, CeO_2 is also studied for various catalytic reactions as it has high oxygen-storing capability and redox character.[9−12] This is the reason why it has been mostly used in oxidation reactions for a long time. However, only CeO_2 as a catalyst is not an ideal choice for achieving the desirable activity. Electronically, Ce−O exists in a redox pair (Ce^{3+}/Ce^{4+}), which oscillates as $Ce^{4+} \leftrightarrow Ce^{3+}$ during the catalytic process to display a redox phenomenon. The modification of CeO_2 with other metal oxides generates more surface reactivity by increasing the adsorption capacity and enhancing its redox property. Additionally, incorporating a precious metal in CeO_2 is another route

Received: April 25, 2024
Revised: July 10, 2024
Accepted: July 11, 2024
Published: July 18, 2024

© 2024 American Chemical Society

https://doi.org/10.1021/acs.langmuir.4c01544
Langmuir 2024, 40, 15721−15730

Scheme 1. Schematic Representation of the NO−CO Catalytic Reaction Setup

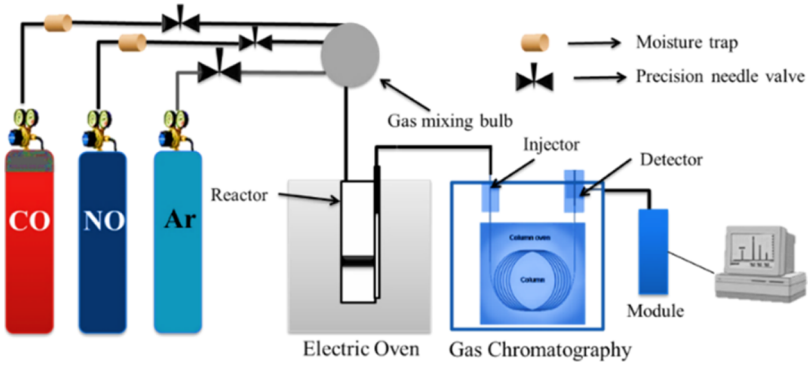

that can contribute significantly to the enhancement of catalytic performance by exerting a higher electronic property that triggers the adsorption and redox behavior.[13,14] Such effect of precious metals has been known for several decades to improve the performance of the host material for catalytic and sensing studies,[15] but developing an ideal combination (with a lower concentration of the precious metal) for achieving the desired target is still a challenging task. Also, in the literature, various reports have demonstrated that CeO_2 and other metal oxides collectively improve the performance of the catalytic reaction. For example, Huang's group reported on Pt-supported CeO_2−TiO_2 and Pt-supported TiO_2 for NO−CO conversion. They observed a greater adsorption of NO and CO and a high electron transfer in the Pt/Ce−Ti catalyst, which later showed significant conversion of NO and CO.[16] Similar other reported combinations such as CeO_2−Al_2O_3,[17] CoO_x/CeO_2,[4] Mn-doped CeO_2,[18] CeO_2−MO_x (0.25) (M = Mn, Fe and Cu),[19] etc. tend to exhibit more synergy and behave as excellent catalytic materials. Further, considering the influence of the precious metal, in our previous report, a promising effect was shown with Pd, wherein increasing amount of Pd assisted in the NO and CO conversion reaction at a lower temperature with a higher conversion yield.[20] Furthermore, Yang et al. reported on the MnOx-CeO_2−Pd/GR catalyst for NO reduction and observed the promising effect of Pd within MnO_x−CeO_2.[21] The $La(Cu_{0.7}Mn_{0.3})_{0.98}M_{0.02}O_3$ (M = Pd, Pt, Ru, Rh) catalyst was reported by Grünbacher et al. for efficient conversion of NO and CO, wherein they were able to modify the electronic structure of the catalytic surface with the introduction of a precious metal.[22]

Like other precious metals, Ru with a specific combination can possess significant catalytic activity in heterogeneous processes. This property is achieved by decorating the surface with Ru for developing active sites, which in turn help to enhance the chemisorption and dissociative property. In ethanol steam reforming studies over M/CeO_2/YSZ (M = Pd, Ag, Ru), Ines A. Carbajaland Ramos' group demonstrated the promising performance of the Ru-composed CeO_2/YSZ catalyst even in the presence of coke, which in other cases is the reason for the catalyst deactivation.[23] Moreover, Karatas et al. showed a significant enhancement in the hydrogen generation on Ru NPs@nano-CeO_2.[24]

In the present study, we have chosen Ru as dopant in the CeO_2 lattice to enhance the performance of the NO−CO reaction. A very few reports of Ru−CeO_2 combination are found in the literature and, to the best of our knowledge, no report on Ru-substituted CeO_2 has been reported for NO−CO reaction. This paper discusses the modification of the cerium oxide catalyst with Ru for converting NO to N_2 and CO to CO_2 efficiently. Further, the detailed characterization of the catalysts has been presented through XRD, XPS, SEM, TEM, and BET surface area. Also, changes in surface properties were monitored using TPD and TPR studies, and using those experimental data, a mechanistic pathway of NO−CO conversion reaction was proposed.

EXPERIMENTAL SECTION

Preparation of the Catalyst. *$Ce_{1-x}Ru_xO_2$ (x = 0, 0.01, 0.025, and 0.05).* The tartaric-acid-assisted solution combustion preparative route was employed to synthesize Ru-substituted CeO_2 series.[25] First and foremost, stoichiometric amounts of $Ce(NH_4)_2(NO_3)_6$ (Sigma-Aldrich) and $RuCl_3$ (Sigma-Aldrich) were dissolved in double distilled water. Further, in the resultant mixture, a weighed amount of tartaric acid was added with vigorous stirring and kept on a hot plate equipped with a stirrer until the solution transformed to gel. The obtained gel was later combusted at 220 °C in an electric oven and finally kept for calcination at 500 °C for 4 h to produce 1, 2.5, and 5% ruthenium-substituted cerium oxide. The catalysts were formulated as $Ce_{0.99}Ru_{0.01}O_2$, $Ce_{0.975}Ru_{0.025}O_2$, and $Ce_{0.95}Ru_{0.05}O_2$, respectively.

Characterization. The recording of X-ray powder diffraction patterns was done on a RIGAKU ULTIMA IV diffractometer with a scanning step of 0.02°. Cu Kα having a wavelength of 1.5418 Å was used as a source of radiation. A Zeiss EVO 18 scanning electron microscope (SEM) was employed for understanding the surface morphology and a Jeol/JEM 2100 high-resolution transmission electron microscopy (HRTEM) instrument was used for determining the nano nature of the prepared oxide. The BET surface area measurements were carried out by N_2 sorption at liquid nitrogen temperature on a QUANTACHORME AUTOSORB iQ-MP-C instrument. A heat treatment of 200 °C was given to the sample to degas the surface adsorbed species. The same instrument is also equipped for temperature-programmed studies such as H_2-TPR, CO-TPD, NO-TPD, and NH_3-TPD, which were done in a quartz reactor from room temperature to 450 °C. Prior to the temperature-programmed studies, samples were heated to 250 °C in a He atmosphere. Spectral data for determining the oxidation state of the elements present in the catalyst were determined using X-ray photoelectron spectroscopy on a PHI 5000 versa probe II spectrophotometer.

Catalytic Study. A schematic representation of the catalytic study is displayed in Scheme 1. Catalytic conversion of NO with CO was studied in a continuous-flow fixed-bed glass reactor system. Around 900 mg of powdered catalyst was loaded between two glass wool plugs. The reactant gases such as nitric oxide (NO) and carbon monoxide (CO) were prepared in the laboratory with a standard preparative route (provided in Supporting Information) and purified by passing through several traps. The other gases like nitrogen (99.9%), argon (99.99%), and hydrogen were used from a commercial pure source. In the reacting chamber, the feed gas containing 5% NO and 5% CO in 90% Ar with a flow rate of 5000 mL h^{-1} was allowed to pass over the catalyst bed using a mass flow meter. Before proceeding with the catalytic test, the catalyst

https://doi.org/10.1021/acs.langmuir.4c01544
Langmuir 2024, 40, 15721−15730

was heated in a nitrogen atmosphere so as to remove any adsorbed species from the catalyst surface. Later, the online monitoring of the reactants and products was done by online Gas chromatogram equipped with TCD detector. For the separation of the gases, a column such as Porapak Q and molecular sieve 13X were employed and analyzed with a TCD detector.

RESULTS AND DISCUSSION

Structural and Surface Characterization. The crystallinity and phase formation of the Ru-substituted CeO_2 were determined via the powder X-ray diffraction pattern and are depicted in Figure 1. All of the prepared compounds show peaks

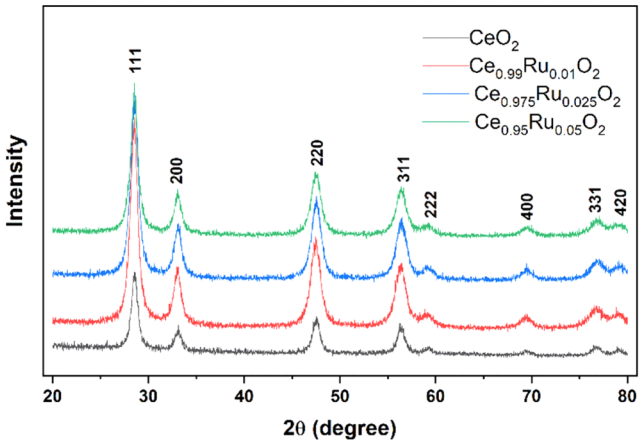

Figure 1. XRD pattern of CeO_2 and Ru-substituted CeO_2 ($Ce_{1-x}Ru_xO_2$) (x = 0.0, 0.01, 0.025, and 0.05).

at 2θ = ~28.51, ~33.01, ~47.55, ~56.23, ~59.23, ~69.33, ~76.75, and ~79.06°, which can be indexed for (111), (200), (220) (311), (222), (400), (331), and (420), respectively. Even after incorporation of Ru, the diffraction pattern of CeO_2 remained identical to that of pure CeO_2, suggesting the formation of monophasic CeO_2 with the same crystal structure, which also matched with the standard JCPDS data card 00-034-0394.[26−28]

This indicates the absence of extra reflection of the Ru species, making Ru-substituted CeO_2 perfectly identical to the monophasic compound. Further, the average crystallite sizes of all of the samples were calculated using Scherer's equation, which were in the range of 10−8 nm. The data pertaining to the same is given in Table 1.

Table 1. Average Crystallite Size and BET Surface Area of $Ce_{1-x}Ru_xO_2$ (0.0, 0.01, 0.025, and 0.05)

catalyst	average crystallite size (nm)	BET surface area (m^2/g)	pore volume (cc/g)	pore diameter (nm)
CeO_2	10	83	0.167	3.8
$Ce_{0.99}Ru_{0.01}O_2$	8	121	0.232	3.4
$Ce_{0.975}Ru_{0.025}O_2$	8	91	0.180	3.0
$Ce_{0.95}Ru_{0.05}O_2$	9	51	0.060	4.1

To gain sufficient idea about how the catalyst appeared at microscopic level, a detailed morphological view of $Ce_{0.95}Ru_{0.05}O_2$ was obtained using SEM. Figure 2a shows the microscopic view at 2 μm and 200 nm scale. By a careful evaluation of the image, it was observed that the particles formed during the preparation were not only in the nano range but also caused a well-arranged porous morphology. This appearance of $Ce_{0.95}Ru_{0.05}O_2$ at a lower scale was a consequence of the adopted preparative route, wherein the evolution of the gases during the preparation of $Ce_{0.95}Ru_{0.05}O_2$ created porous channels.[26] A further in-depth microscopic view of $Ce_{0.95}Ru_{0.05}O_2$ was taken using high-resolution transmission electron microscopy (HRTEM) for understanding the sample surface property at nano range scale. The same image is depicted in Figure 2b. The microscopic view at 10 nm scale confirmed the existence of nanoparticles showing a somewhat agglomerated spherical and cylindrical appearance. Also, a histogram of the particle sizes shows the dispersion below 10 nm having the highest density of particle size from 5 to 6 nm range.

In the N_2 sorption study, all of the samples in the series showed a similar N_2 adsorption−desorption isotherm. The data related to the N_2 sorption studies are presented in Figure 3. From Figure 3, it can be seen that the isotherm of the prepared oxides appears as a Type II isotherm, which is in accordance with IUPAC classification.[26,29] The values of BET surface area of all of the studied catalysts are given in Table 1. Introduction of 1% Ru showed an increase in the surface area, but further increase of the Ru concentration in CeO_2 led to a reduction in surface area. This increase may be due to the formation of more pore volume in $Ce_{0.99}Ru_{0.01}O_2$ and a lower pore volume in $Ce_{0.95}Ru_{0.05}O_2$, thereby dropping off its overall surface area as seen in Table 1. For gathering a clear idea about the pores, a BJH pore size distribution curve was generated from the N_2 sorption study (Figure S1).

From the BJH profile, it was then confirmed that the increase in size of $Ce_{0.99}Ru_{0.01}O_2$ is mainly due to increment in the pore volume, which is in conformity with Table 1.

XPS analyses were conducted in order to understand the chemical valence states of the elements present in $Ce_{0.95}Ru_{0.05}O_2$. All of the spectra were fitted with Gaussian−Lorentz curve fitting method. As seen in Figure 4, the peaks showed a binding energy similar to that of Ce, Ru, and O, thus confirming the existence of Ce, Ru, and O in the analyzed sample. Also, based on the XPS analyses, the percentages of $Ce^{4+/3+}$, Ru^{4+}, and the defect oxygen in various oxide structures are summarized in Table S1.

The Ce 3d spectrum of $Ce_{0.95}Ru_{0.05}O_2$ shows the presence of Ce^{4+} and Ce^{3+} as depicted in Figure 4a. The Ce 3d spectrum was fitted with Gaussian−Lorentz fitting, which showed eight photoelectrons splitting. In the observed peaks, the $3d_{5/2}$ spin orbit state was labeled as "v" and $3d_{3/2}$ orbital states were denoted by the "u" symbol. Ce is often observed as an important component due to its typical redox pair. The peaks labeled as v′ and u′ were attributed to the +3 state of Ce and the remaining six photoemission peaks (i.e., v, v″, v‴, u, u″, and u‴) confirm the presence of Ce^{4+} state.[30,31] Generally, the existence of both Ce^{3+} and Ce^{4+} is well known.[32] Figure 4b shows the Ru 3d spectra along with C 1s peak. The existence of Ru species was clearly identified by the peak fitting procedure, wherein the presence of Ru^{4+} was revealed.[31,33] The XPS spectrum of O 1s is shown in Figure 4c and various kinds of oxygen present were investigated. The main peak appearing at a lower binding energy i.e., 529 eV, is attributed to the lattice oxygen and the oxygen that appears at a higher binding energy, 531.22 eV, is considered to be due to the surface defect.[34] Based on the percentage calculations, Ce^{4+} was observed to be present in a higher concentration and, also, Ce^{3+} was present to quite a larger extent, which is essential for the redox reaction.

https://doi.org/10.1021/acs.langmuir.4c01544
Langmuir 2024, 40, 15721−15730

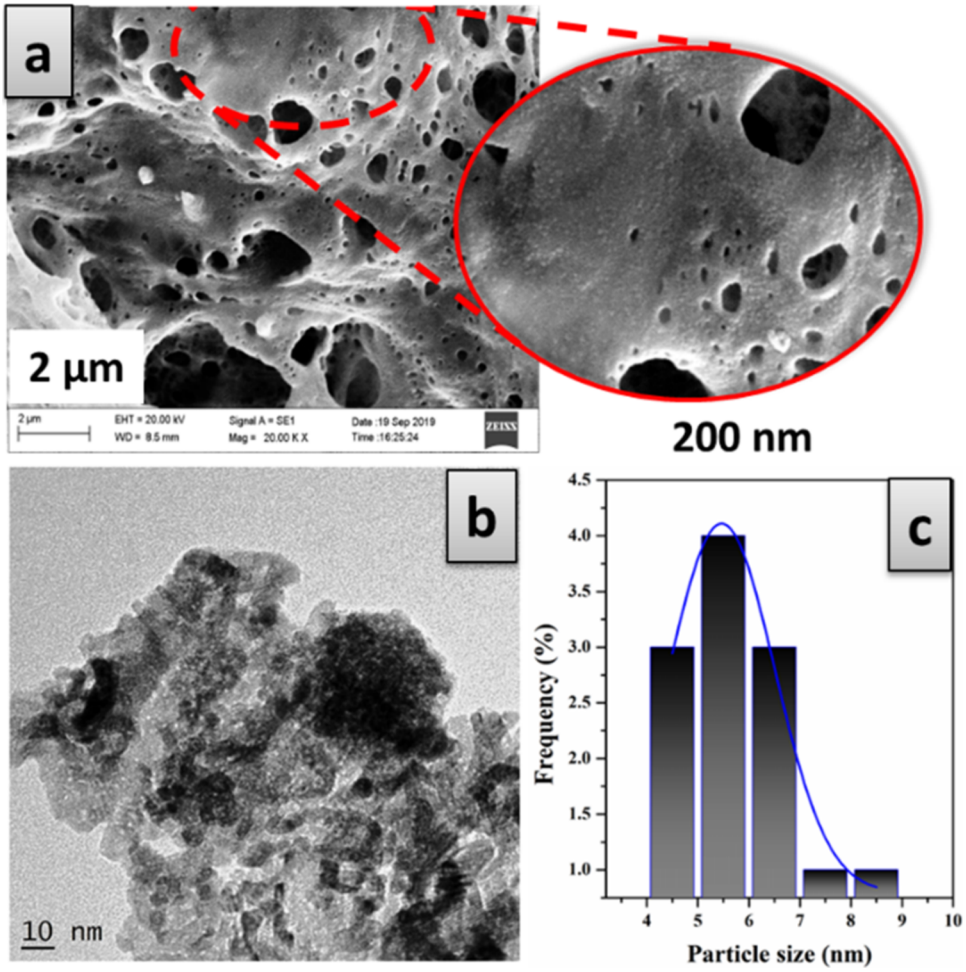

Figure 2. SEM (a), HRTEM image (b), and particle size distribution (c) of $Ce_{0.95}Ru_{0.05}O_2$.

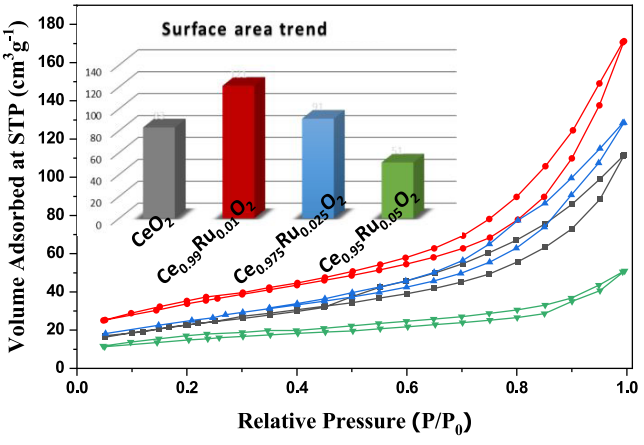

Figure 3. N_2 adsorption−desorption isotherm of $Ce_{1-x}Ru_xO_2$ (x = 0.0, 0.01, 0.025, and 0.05).

Surface Desorption Studies of NH_3, CO, and NO. The influence of ruthenium with respect to the surface acidic property of cerium oxide has been investigated with ammonia desorption studies. Figure 5 shows the NH_3-temperature-programmed desorption (NH_3-TPD) patterns of CeO_2, $Ce_{0.99}Ru_{0.01}O_2$, and $Ce_{0.95}Ru_{0.05}O_2$. In CeO_2, three desorption peaks of ammonia are observed residing at 130, 340, and 430 °C, which can be ascribed to the weak acidic, medium acidic, and strong acidic sites, respectively. After substitution of 1% Ru in CeO_2, an increase in ammonia-ceria chemisorption strength was observed, which ultimately resulted in a lesser desorption of NH_3 at a lower temperature. Further, a higher amount of strong acidic sites in $Ce_{0.99}Ru_{0.01}O_2$ has been observed, indicating both strong and weak acidic sites. However, in $Ce_{0.95}Ru_{0.05}O_2$, continuous desorption of ammonia has been observed, which shows the presence of acidic character in the entire studied temperature. This means the catalyst surface has the tendency to form chemical bonds with the electron-donating reacting species in a wide temperature range. The acidity influences the adsorption and activation of CO molecules on the surface of the catalyst as acidic sites have more affinity toward the CO molecule and help in removing the surface lattice oxygen to form CO_2. The continuous desorption of ammonia suggests dynamic acidity, which could affect the NO−CO conversion and can be correlated to a higher conversion of $Ce_{0.95}Ru_{0.05}O_2$. Since CeO_2 did not show any significantly strong acidic sites at lower temperatures compared to other catalysts, it therefore may be unfavorable for the NO−CO reaction.

Further, the collective surface reactivity of CO is essential to understand the interaction of CO with the catalyst surface. Figure 6 represents the CO-TPD profile of the Ru-substituted CeO_2 series. In the TPD profile, the desorption of chemisorbed CO produces two peaks, out of which one is positioned in a lower-temperature region (from 50 to 125 °C) and the other in a higher-temperature region (from 250 to 350 °C). The peak originated at lower temperature can be attributed to the weakly

https://doi.org/10.1021/acs.langmuir.4c01544
Langmuir 2024, 40, 15721−15730

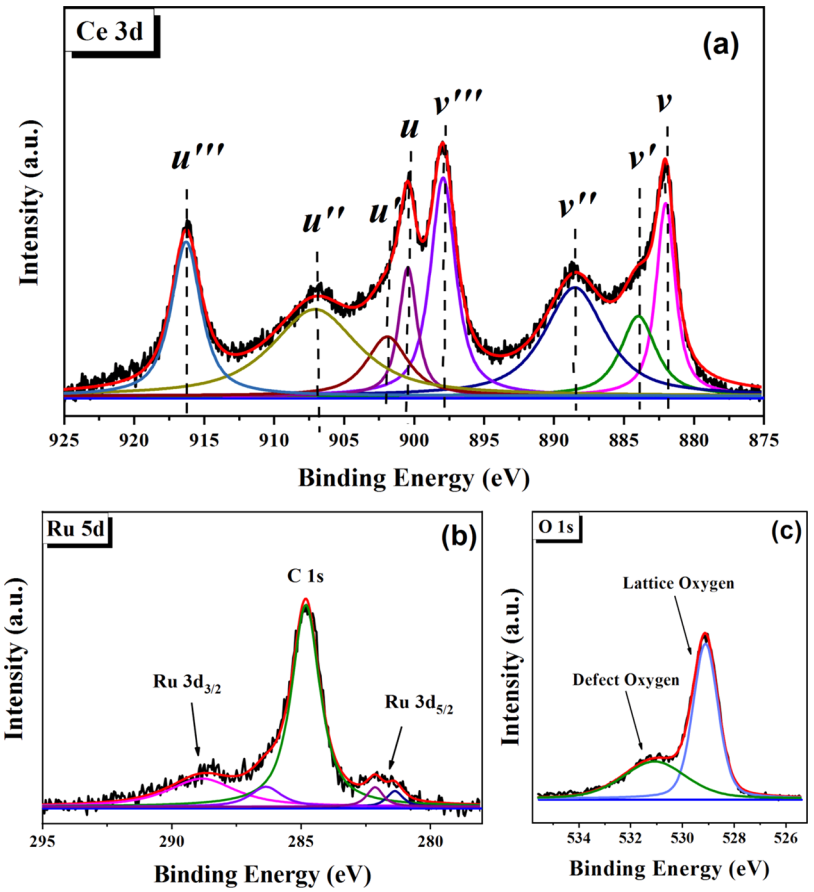

Figure 4. XPS spectra of (a) Ce 3d, (b) Ru 5d, and (c) O 1s from $Ce_{0.95}Ru_{0.05}O_2$.

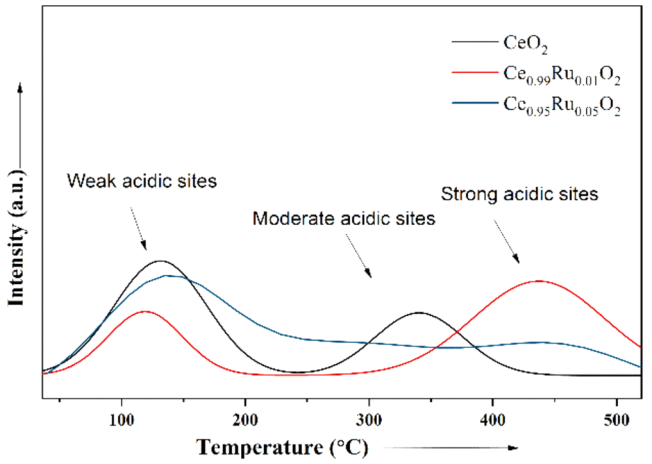

Figure 5. NH_3 temperature-programmed esorption studies over CeO_2, $Ce_{0.99}Ru_{0.01}O_2$, and $Ce_{0.95}Ru_{0.05}O_2$.

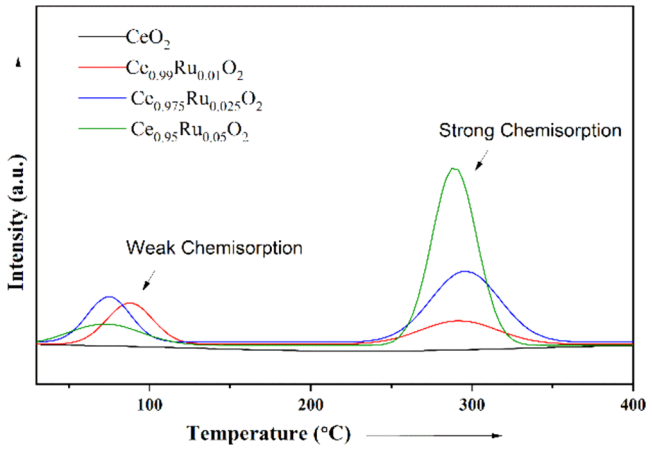

Figure 6. CO-temperature-programmed desorption studies over CeO_2, $Ce_{0.99}Ru_{0.01}O_2$ $Ce_{0.975}Ru_{0.025}O_2$, and $Ce_{0.95}Ru_{0.05}O_2$.

chemisorbed CO and the one at higher temperature is associated with the strongly chemisorbed CO.[35] Thus, it is evident that the two different chemisorption sites differ in strength with respect to the CO bonding. For pure CeO_2, the absence of a desorption peak clarifies the lack of CO's affinity toward the adsorption and reaction, while, with the addition of Ru in cerium oxide, improvement in the adsorption of CO is observed and is later found to increase linearly with increase in the Ru concentration. This result can also provide a more significant insight into the NO−CO reaction pathway. Since CO is more strongly adsorbed on the catalyst surface, it thus confirms the availability of the CO during the catalytic process. From the prepared series, the quantum of CO chemisorbed on $Ce_{0.95}Ru_{0.05}O_2$ showed a higher concentration as compared to other catalysts from the series and the order of CO desorption is observed as $Ce_{0.95}Ru_{0.05}O_2$ > $Ce_{0.975}Ru_{0.025}O_2$ > $Ce_{0.99}Ru_{0.01}O_2$ > CeO_2. In fact, CeO_2 showed no adsorption of CO on the surface, but showed improved drastic adsorption capacity only on Ru incorporation. This suggests alteration of the surface and electronic properties of CeO_2 with Ru, creating active sites that facilitate stronger interactions with the CO molecules. Therefore, the presence of

https://doi.org/10.1021/acs.langmuir.4c01544
Langmuir 2024, 40, 15721−15730

Ru significantly improves the overall performance of cerium oxide.

Knowledge of surface NO reactivity is also essential for determining the process of the catalytic NO−CO reaction. Here, desorption of NO was studied on $Ce_{0.99}Ru_{0.01}O_2$ and $Ce_{0.95}Ru_{0.05}O_2$ in the temperature range of 30−475 °C and the respective TPD profile is given in Figure 7. The TPD studies

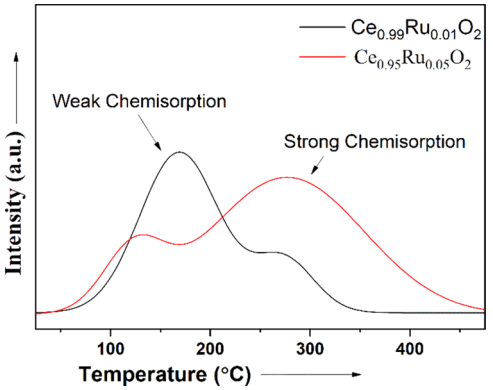

Figure 7. NO-temperature-programmed desorption studies over $Ce_{0.99}Ru_{0.01}O_2$ and $Ce_{0.95}Ru_{0.05}O_2$.

showed desorption of chemisorbed NO from both of the Ru-doped catalysts. The presence of different chemisorption sites always differs depending on the catalyst surface and NO adsorption strength. Both of the studied catalysts showed the adsorption of NO on the catalyst surface. The desorption profile of $Ce_{0.99}Ru_{0.01}O_2$ depicts strong as well as weak NO chemisorption sites, but the amount of weakly adsorbed NO was observed to be higher as compared to that of the strongly adsorbed NO. However, increasing the concentration of Ru holds the NO more tightly toward the surface, as demonstrated by the higher-intensity peak in the higher-temperature region. This shows that the surface can also hold the NO molecule by donating its electron to the π^* of the NO molecule. One potential approach, as demonstrated by Abujarada and colleagues, suggests that the interaction of NO with a metal surface involves the transfer of electrons from the substrate to the $2\pi^*$ orbital of NO, thereby influencing the strength of the N−O bond.[36] On the other hand, CO will be chemisorbed on the catalyst surface by donating the electron to the surface and this quantum of CO adsorption increases as the number of Lewis sites increases.[37]

Surface Reduction Studies with H_2. The reduction patterns of CeO_2 and Ru-substituted catalysts are displayed in Figure 8. The pure cerium oxide exhibits a reduction peak at around 245 °C, which may correspond to the easily reducible cerium species from the CeO_2 structure.[26,38] The incorporation of 1% Ru in CeO_2 showed a remarkable improvement in its surface reduction pattern, which has been indicated by the two reduction peaks at 117 and 143 °C. Also, in $Ce_{0.975}Ru_{0.025}O_2$, a change in M−O strength can be inferred, which creates the sharp reduction peak at 96 °C due to increasing oxygen mobility because of the presence of more Ru species. The incorporation of Ru species into CeO_2-based catalysts has a notable impact on oxygen mobility and catalytic performance. Studies indicate that the introduction of ruthenium enhances the reactivity of the catalyst, leading to the formation of Ru−O−Ce bonds, which are essential for catalytic oxidation reactions.[39]

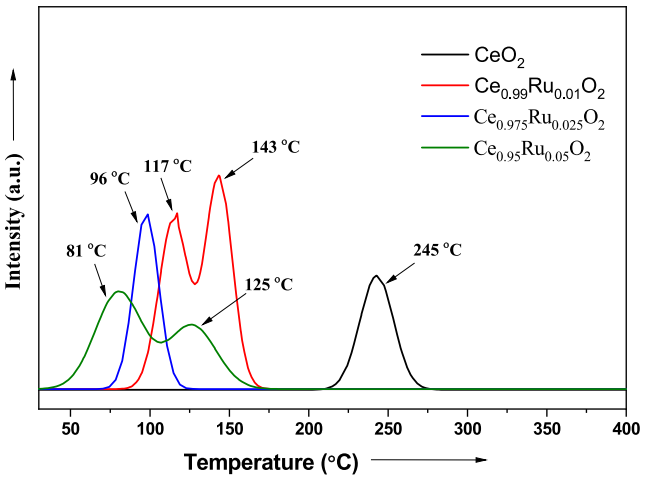

Figure 8. H_2-temperature-programmed reduction studies over $Ce_{1-x}Ru_xO_2$ (x = 0.01, 0.025, and 0.05).

Further, increase in the Ru in ceria ($Ce_{0.95}Ru_{0.05}O_2$) showed the highest oxygen release at 81 and 125 °C, which was observed to be a great achievement obtained within the series of the catalysts prepared with respect to temperature. This shifting of the reduction pattern by addition of Ru is mainly due to weakening of Ce−O bond on Ru doping, which alters the mobility of oxygen and also its redox character.[40] The increase in oxygen mobility with respect to temperature is in the order of $Ce_{0.95}Ru_{0.05}O_2$ > $Ce_{0.975}Ru_{0.025}O_2$ > $Ce_{0.99}Ru_{0.01}O_2$ > CeO_2. CeO_2 showed a higher binding energy for the removal of O_2 and therefore the mobility of O_2 is highly restricted. After incorporation of Ru, the mobility of O_2 requires a lesser amount of energy, which subsequently results in a highly redox surface.

Catalytic Performance. *NO−CO Redox Conversion.* The catalytic reaction of NO and CO simultaneously over Ru-substituted CeO_2 has been studied, and the results are presented in terms of percent CO and NO conversion in Figure 9. The obtained result clearly indicates the promising effect of ruthenium-incorporated CeO_2 for catalytic redox reaction of NO and CO. Pure cerium oxide showed unresponsive behavior with respect to NO−CO catalytic conversion, wherein no conversion of NO and CO was observed in the temperature range of 30−250 °C. Such response is obvious in CeO_2, as it

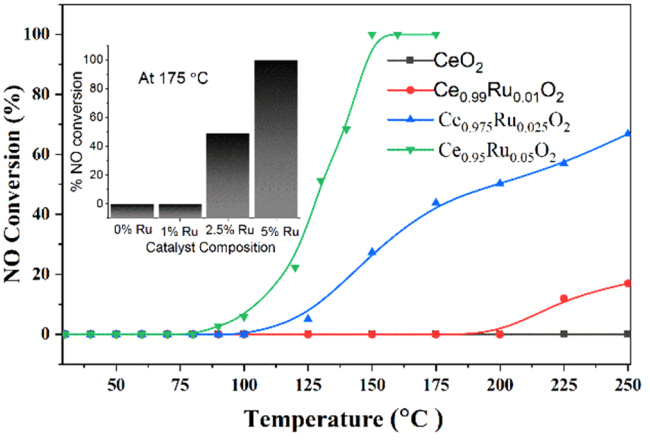

Figure 9. NO % conversion studies from the CO-NO redox reaction over CeO_2, $Ce_{0.99}Ru_{0.01}O_2$, $Ce_{0.975}Ru_{0.025}O_2$, and $Ce_{0.95}Ru_{0.05}O_2$ (5% NO and 5% CO in Ar at a flow rate of 5000 mL h^{-1}).

https://doi.org/10.1021/acs.langmuir.4c01544
Langmuir 2024, 40, 15721−15730

requires a higher activation energy to take part in the NO−CO catalytic process. Also, from the literature studies, it is clear that the reduction of NO on CeO_2 is initiated above 250 °C.[41] However, the catalytic activity of CeO_2 was found to increase gradually by the addition of Ru. In the case of $Ce_{0.99}Ru_{0.01}O_2$, addition of 1% Ru showed 19% NO−CO conversion at 250 °C and this conversion rate was increased up to 70% as the concentration of Ru was increased ($Ce_{0.975}Ru_{0.025}O_2$). Further, improved NO−CO conversion ability is achieved by $Ce_{0.95}Ru_{0.05}O_2$, showing 100% conversion at 150 °C, which is the highest amount among the series of catalysts prepared. The trend observed in NO−CO catalytic conversion can be represented as CeO_2 < $Ce_{0.99}Ru_{0.01}O_2$ < $Ce_{0.975}Ru_{0.025}O_2$ < $Ce_{0.95}Ru_{0.05}O_2$. Such improvement in the catalytic conversion can be directly related to the advanced effect of electron-rich Ru when it is added to the CeO_2 system, thereby providing effective synergy in the catalytic process. The addition of Ru to CeO_2 can lead to the formation of atomically dispersed Ru ions on ceria surfaces, creating unique catalytic properties with high stability and redox reactions. Also, Carlotto et al. suggested unique catalytic properties of Ru, responsible for its high surface reactivity and affinity for CO, which are pivotal in facilitating the catalytic conversion of NO and CO at lower temperatures.[42] This synergetic interaction affects the ratio of NO and CO adsorption on the surface, which can be seen from the NO and CO TPD results. The trend of NO and CO desorption followed a similar pattern to that of the catalytic activity as availability of a higher amount of NO and CO leads to a higher conversion rate. After Ru incorporation in CeO_2, the oxygen mobility increased at lower temperatures and this may be also contributing to the NO−CO reaction activity.

In addition, N_2O formation was also observed over the catalysts, and the chromatogram for the same is depicted in Figure S3. N_2O is one of the products that are mostly produced in a lower-temperature region as a result of partial reduction of the NO molecule. Here, a minimum amount of N_2O was seen over $Ce_{0.95}Ru_{0.05}O_2$ during the entire reaction. Further, the catalyst also showed a significantly stable activity and reusability in regard to the NO−CO redox reaction. The plot of stability and recyclability is depicted in Figures S4 and S5. The reaction stability over $Ce_{0.95}Ru_{0.05}O_2$ was studied at 175 °C for 6 h, which was found to be good and to maintain the 100% conversion rate.

Mechanism for the NO−CO Reaction. The mechanism for the reduction of NO using various reducing gases has been reported by several research groups giving various theoretical and experimental approaches.[2,43−45] Studies showed that the redox conversion of NO and CO on the catalyst surface could proceed via the Langmuir−Hinshelwood (L−H) mechanism and also with the Eley−Rideal (E−R) mechanism.[6,46,47] Another mechanism is the Mars-van Krevelen (MVK)-type mechanism, which decides the reaction pathway in most of the oxidation reactions.[48−50] Generally, the L−H mechanism is a universally accepted mechanism for the NO−CO reaction, wherein both NO and CO get adsorbed on the surface of the catalyst during the catalytic conversion process. Nevertheless, the possibility to have more than one type of mechanism on a single catalytic material for a particular reaction is also universally accepted as the surface of the catalyst processes variable active sites.

The probable mechanism for the NO−CO redox reaction was proposed with the help of NO and CO desorption and other studies. Since CO and NO showed desorption in higher-temperature regions, the availability of both the reactants is thus confirmed on the catalyst surface, and probable pathways for NO−CO reaction are given in Scheme 2. Here, $MO_{(S)}$ represents the active site involved in CO adsorption and $MO_{(S')}$ signifies the active site for NO adsorption for simplicity. In the proposed mechanism, adsorption of CO (eq 1) followed by the adsorption of NO molecule (eq 2) is the first step of the reaction. Based on the experimental findings of NO/CO TPD studies, the availability of the reactants was observed on the catalyst surface. This availability thus supports the L−H type pathways to confirm the simultaneous conversion of NO and CO. In the third step, as the temperature ramps up, the adsorbed CO will react with the adsorbed NO on the catalyst surface (eq 3). The simultaneous weakening of the N−O bond and formation of the stronger O−CO take place, which further may lead to N_2 and CO_2 formation as shown in eq 5. Since Ru-doped CeO_2 showed a surface reduction pattern, easy removal of

Scheme 2. Proposed Reaction Mechanism Pathway of NO Reduction by CO

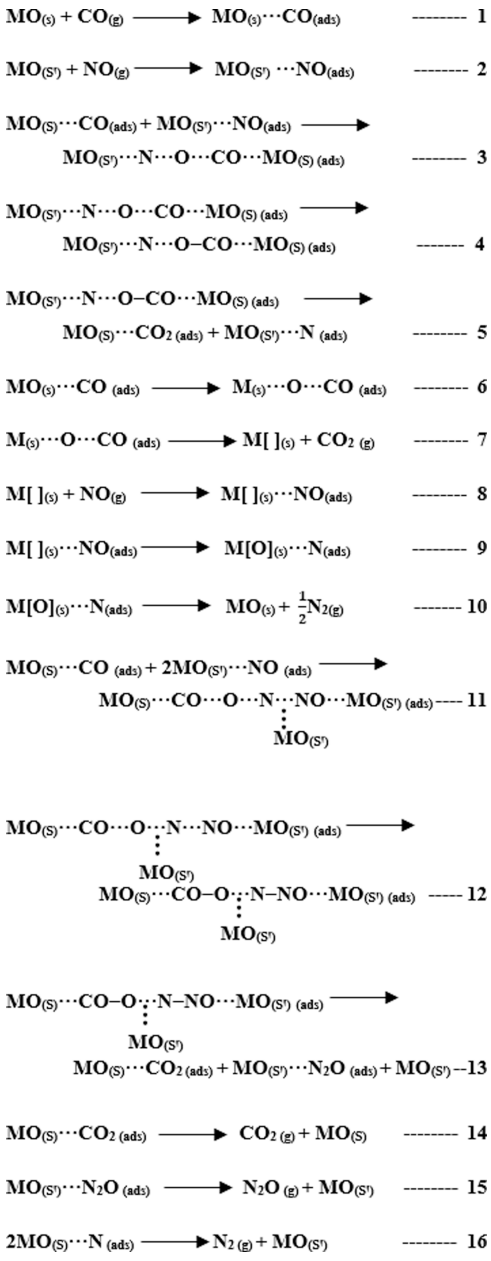

https://doi.org/10.1021/acs.langmuir.4c01544
Langmuir 2024, 40, 15721−15730

oxygen was facilitated from the catalyst surface at a lower temperature. This may also help in the NO/CO redox reaction, which can proceed with the MVK-type mechanism as shown below. CO adsorption over the catalyst surface consumes the lattice oxygen to form CO_2, making the surface oxygen deficient (eqs 6 and 7). Later, this oxygen-deficient surface site acts as an active site for NO adsorption and subsequently can be regenerated by the oxygen from the NO molecule, releasing N_2 back to the atmosphere as depicted in eqs 8−10. In addition to N_2 and CO_2, N_2O was also detected in the system during the initial period of the reaction. This can be explained as follows: when CO forms a partially weak bonding with the adsorbed NO, there can be the possibility that the available neighboring adsorbed NO will also react simultaneously with the same NO molecule (eq 11), where breaking and construction of new bonds occur, which may lead to the formation of CO_2 and N_2O as shown in eqs 12 and 13. Finally, as described in eqs 14−16, desorption of the formed gases (N_2, CO_2, and N_2O) takes place, leaving the active site for the next catalytic cycle. This mechanistic pathway is partly in agreement with the reported mechanism in the literature.[43,51]

Since both the gases, i.e., NO and CO, showed adsorption on the Ru-doped catalyst by TPD studies, the mechanism could proceed via the L−H mechanism (eqs 1−5). Also, TPR reduction studies showed oxygen mobility at a lower temperature in the Ru-doped catalyst and are therefore also expected to show MVK mechanisms (eqs 6−10). Furthermore, subsequent equations showed the formation of products such as CO_2, N_2, and N_2O.

CONCLUSION

This study demonstrates the fabrication of cerium oxide using ruthenium (Ru) for catalyzing the conversion of NO and CO to N_2 and CO_2, respectively. Monophasic Ru-substituted CeO_2 materials were developed through a tartaric-acid-assisted solution combustion method, resulting in porous nanomaterials with high surface areas. The stronger interaction between Ru and Ce indicated enhancement in the surface reducibility of the catalyst and, with the increasing Ru concentration, the shifting of the reduction point to a lower temperature has been observed. In addition to this, the strong interaction between these active metals is able to produce both Lewis acidic sites as well as Lewis basic sites within the catalyst, which are very much essential for the sorption of CO and NO. Further, catalytic results displayed the conversion of NO−CO over all of the Ru-modified CeO_2. However, significant enhancement was only achieved on $Ce_{0.95}Ru_{0.05}O_2$, which could achieve 100% conversion of NO and CO at 150 °C. This lower-temperature conversion is thus justified as a high synergistic interaction generated with the Ru, which creates more adsorption sites for CO, resulting in a CO-enriched catalyst surface. Interestingly, it has been observed that both NO and CO react after the formation of metal-NO and metal-CO bonds on the catalyst surface. Finally, with all of the experimental evidence, a Langmuir−Hinshelwood and Mars-Van Krevelen-type mechanism has been proposed for the NO−CO redox reaction, which very well directs the catalytic reaction when both the reactants show an affinity toward the surface, forming a chemical bond.

ASSOCIATED CONTENT

Supporting Information

The Supporting Information is available free of charge at https://pubs.acs.org/doi/10.1021/acs.langmuir.4c01544.

Preparation of gases (CO and NO), Percent NO and CO conversion formula, Detailed description of TPR and TPD experimentation, Percentage determination of elements through XPS, BJH pore size distribution study, CO conversion plot from NO−CO catalytic studies, Chromatogram of CO_2 and N_2O formation, Stability study, Recyclability studies. (PDF)

AUTHOR INFORMATION

Corresponding Authors

Rahul D. Kerkar − *School of Chemical Sciences, Goa University, Panaji 403206 Goa, India; P.E.S.'s S. R. S. N. College of Arts and Science, Farmagudi 403401 Goa, India;* orcid.org/0000-0003-2436-0572; Email: rahulkerkar27@gmail.com

Arun.V. Salker − *School of Chemical Sciences, Goa University, Panaji 403206 Goa, India*; Email: sav@unigoa.ac.in

Complete contact information is available at: https://pubs.acs.org/10.1021/acs.langmuir.4c01544

Author Contributions

The manuscript was written through the contributions of all authors. All authors have given approval to the final version of the manuscript.

Notes

The authors declare no competing financial interest.

ACKNOWLEDGMENTS

The authors sincerely thank UGC-CSIR NET-JRF for the financial assistance.

ABBREVIATIONS

MVK, Mars-van Krevelen; L−H, Langmuir−Hinshelwood

REFERENCES

(1) Zhdanov, V. P.; Kasemo, B. Mechanism and Kinetics of the NO-CO Reaction on Rh. *Surf. Sci. Rep.* **1997**, *29* (2), 31−90.

(2) Liu, T.; Yao, Y.; Wei, L.; Shi, Z.; Han, L.; Yuan, H.; Li, B.; Dong, L.; Wang, F.; Sun, C. Preparation and Evaluation of Copper-Manganese Oxide as a High-Efficiency Catalyst for CO Oxidation and NO Reduction by CO. *J. Phys. Chem. C* **2017**, *121* (23), 12757−12770.

(3) Sierra-Pereira, C. A.; Urquieta-González, E. A. Reduction of NO with CO on CuO or Fe_2O_3 Catalysts Supported on TiO_2 in the Presence of O_2, SO_2 and Water Steam. *Fuel* **2014**, *118*, 137−147.

(4) Savereide, L.; Nauert, S. L.; Roberts, C. A.; Notestein, J. M. The Effect of Support Morphology on CoO_X/CeO_2 Catalysts for the Reduction of NO by CO. *J. Catal.* **2018**, *366*, 150−158.

(5) Wan, H.; Li, D.; Dai, Y.; Hu, Y.; Liu, B.; Dong, L. Catalytic Behaviors of CuO Supported on Mn_2O_3 Modified γ-Al_2O_3 for NO Reduction by CO. *J. Mol. Catal. A* **2010**, *332* (1−2), 32−44.

(6) Boningari, T.; Pavani, S. M.; Ettireddy, P. R.; Chuang, S. S. C.; Smirniotis, P. G. Mechanistic Investigations on NO Reduction with CO over Mn/TiO_2 Catalyst at Low Temperatures. *Mol. Catal.* **2018**, *451*, 33−42.

(7) Pan, K. L.; Young, C. W.; Pan, G. T.; Chang, M. B. Catalytic Reduction of NO by CO with Cu-Based and Mn-Based Catalysts. *Catal. Today* **2020**, *348* (300), 15−25.

(8) Theerthagiri, J.; Park, J.; Das, H. T.; Rahamathulla, N.; Cardoso, E. S. F.; Murthy, A. P.; Maia, G.; Vo, D. -V N.; Choi, M. Y. Electrocatalytic Conversion of Nitrate Waste into Ammonia: A Review. *Environ. Chem. Lett.* **2022**, *20* (5), 2929−2949.

(9) Yu, J.; Qin, X.; Yang, Y.; Lv, M.; Yin, P.; Wang, L.; Ren, Z.; Song, B.; Li, Q.; Zheng, L.; Hong, S.; Xing, X.; Ma, D.; Wei, M.; Duan, X. Highly Stable Pt/CeO_2 Catalyst with Embedding Structure toward

Water−Gas Shift Reaction. *J. Am. Chem. Soc.* **2024**, *146* (1), 1071−1080.
(10) Shimizu, K.; Kawachi, H.; Satsuma, A. Study of Active Sites and Mechanism for Soot Oxidation by Silver-Loaded Ceria Catalyst. *Appl. Catal., B* **2010**, *96* (1−2), 169−175.
(11) Hu, Q.; Cao, K.; Lang, Y.; Chen, R.; Chu, S.; Jia, L.; Yue, J.; Shan, B. Improved NO-CO Reactivity of Highly Dispersed Pt Particles on CeO2 Nanorod Catalysts Prepared by Atomic Layer Deposition. *Catal. Sci. Technol.* **2019**, *9* (10), 2664−2672.
(12) Nolan, M.; Parker, S. C.; Watson, G. W. CeO_2 Catalysed Conversion of CO, NO_2 and NO from First Principles Energetics. *Phys. Chem. Chem. Phys.* **2006**, *8* (2), 216−218.
(13) Trovarelli, A. Catalytic Properties of Ceria and CeO_2- Containing Materials. *Catal. Rev.* **1996**, *38* (4), 439−520.
(14) Hegde, M. S.; Bera, P. Noble Metal Ion Substituted CeO_2 Catalysts: Electronic Interaction between Noble Metal Ions and CeO_2 Lattice. *Catal. Today* **2015**, *253*, 40−50.
(15) Naik, S. S.; Lee, S. J.; Theerthagiri, J.; Yu, Y.; Choi, M. Y. Rapid and Highly Selective Electrochemical Sensor Based on ZnS/Au-Decorated F-Multi-Walled Carbon Nanotube Nanocomposites Produced via Pulsed Laser Technique for Detection of Toxic Nitro Compounds. *J. Hazard. Mater.* **2021**, *418*, No. 126269.
(16) Huang, K.; Lin, L.; Yang, K.; Dai, W.; Chen, X.; Fu, X. Promotion Effect of Ultraviolet Light on NO+CO Reaction over Pt/TiO_2 and Pt/CeO_2-TiO_2 Catalysts. *Appl. Catal., B* **2015**, *179*, 395−406.
(17) Kantcheva, M.; Samarskaya, O.; Ilieva, L.; Pantaleo, G.; Venezia, A. M.; Andreeva, D. In Situ FT-IR Investigation of the Reduction of NO with CO over Au/CeO_2-Al_2O_3 Catalyst in the Presence and Absence of H2. *Appl. Catal., B* **2009**, *88* (1−2), 113−126.
(18) Deng, C.; Huang, Q.; Zhu, X.; Hu, Q.; Su, W.; Qian, J.; Dong, L.; Li, B.; Fan, M.; Liang, C. The Influence of Mn-Doped CeO_2 on the Activity of CuO/CeO_2 in CO Oxidation and NO + CO Model Reaction. *Appl. Surf. Sci.* **2016**, *389*, 1033−1049.
(19) Bahrami, S.; Niaei, A.; Illán-Gómez, M. J.; Tarjomannejad, A.; Mousavi, S. M.; Albaladejo-Fuentes, V. Catalytic Reduction of NO by CO over CeO_2-MO_x (0.25) (M = Mn, Fe and Cu) Mixed Oxides - Modeling and Optimization of Catalyst Preparation by Hybrid ANN-GA. *J. Environ. Chem. Eng.* **2017**, *5* (5), 4937−4947.
(20) Kerkar, R. D.; Salker, A. V. Nitric Oxide Reduction by Carbon Monoxide and Carbon Monoxide Oxidation by O_2 over Co−Mn Composite Oxide Material. *Appl. Nanosci.* **2020**, *10* (1), 141−149.
(21) Yang, L.; You, X.; Sheng, Z.; Ma, D.; Yu, D.; Xiao, X.; Wang, S. The Promoting Effect of Noble Metal (Rh, Ru, Pt, Pd) Doping on the Performances of MnO_x-CeO_2/graphene Catalysts for the Selective Catalytic Reduction of NO with NH_3 at Low Temperatures. *New J. Chem.* **2018**, *42* (14), 11673−11681.
(22) Grünbacher, M.; Tarjomannejad, A.; Nezhad, P. D. K.; Praty, C.; Ploner, K.; Mohammadi, A.; Niaei, A.; Klötzer, B.; Schwarz, S.; Bernardi, J.; Farzi, A.; Gómez, M. J. I.; Rivero, V. T.; Penner, S. Promotion of $La(Cu_{0.7}Mn_{0.3})_{0.98}M_{0.02}O_{3-\delta}$ (M = Pd, Pt, Ru and Rh) Perovskite Catalysts by Noble Metals for the Reduction of NO by CO. *J. Catal.* **2019**, *379*, 18−32.
(23) Ramos, I. A. C.; Montini, T.; Lorenzut, B.; Troiani, H.; Gennari, F. C.; Graziani, M.; Fornasiero, P. Hydrogen Production from Ethanol Steam Reforming on M/CeO_2/YSZ (M = Ru, Pd, Ag) Nanocomposites. *Catal. Today* **2012**, *180* (1), 96−104.
(24) Karatas, Y.; Gülcan, M.; Sen, F. Catalytic Methanolysis and Hydrolysis of Hydrazine-Borane with Monodisperse Ru NPs@nano-CeO_2 Catalyst for Hydrogen Generation at Room Temperature. *Int. J. Hydrogen Energy* **2019**, *44* (26), 13432−13442.
(25) Kerkar, R. D.; Salker, A. V. Significant Effect of Multi-Doped Cerium Oxide for Carbon Monoxide Oxidation Studies. *Mater. Chem. Phys.* **2020**, *253*, No. 123326.
(26) Kerkar, R. D.; Salker, A. V. A Route to Develop the Synergy Between CeO_2 and CuO for Low Temperature CO Oxidation. *Catal. Lett.* **2020**, *150* (10), 2774−2783.
(27) Sun, Y.; Cop, P.; Djerdj, I.; Guo, X.; Weber, T.; Khalid, O.; Guo, Y.; Smarsly, B. M.; Over, H. CeO_2 Wetting Layer on ZrO_2 Particle with Sharp Solid Interface as Highly Active and Stable Catalyst for HCl Oxidation Reaction. *ACS Catal.* **2019**, *9*, 10680−10693.
(28) Sellers-Antón, B.; Bailon-García, E.; Cardenas-Arenas, A.; Davo-Quiñonero, A.; Lozano-Castello, D.; Bueno-Lopez, A. Enhancement of the Generation and Transfer of Active Oxygen in Ni/CeO_2 Catalysts for Soot Combustion by Controlling the Ni−ceria Contact and the Three-Dimensional Structure. *Environ. Sci. Technol.* **2020**, *54* (4), 2439−2447.
(29) Thommes, M.; Kaneko, K.; Neimark, A. V.; Olivier, J. P.; Rodriguez-Reinoso, F.; Rouquerol, J.; Sing, K. S. W. Physisorption of Gases, with Special Reference to the Evaluation of Surface Area and Pore Size Distribution (IUPAC Technical Report). *Pure Appl. Chem.* **2015**, *87* (9−10), 1051−1069.
(30) Guo, L.; Tian, Y.; Li, J.; Zhao, D.; Yu, X.; Ding, T.; Jiang, Z.; Li, X. Effect of Sn-Rich and Ce-Rich $Sn_{1-x}Ce_xO_2$ Supports of Pd Catalysts on CO Oxidation. *Catal. Today* **2020**, *355*, 358.
(31) Zhou, Y.; Xu, S.; Zhang, Y.; Hu, X.; Li, F.; Chen, X.; Cai, H.; Wang, J.; Shi, L.; Chen, X. Synergistic Effect over a Remarkable Durable and Active Polymetallic Ru-Doped Fe-Co-Ce/γ-Al_2O_3 Nanocatalyst: Interfacial Lewis Acid-Base Pair Dependent Reaction Mechanism for Landfill Leachate. *Chem. Eng. J.* **2020**, *382*, No. 122938.
(32) Zhang, J.; Li, T.; Wang, C. A.; Luo, J. L. The Rational Design of Sandwich-like MnO_2-Pd-CeO_2 Hollow Spheres with Enhanced Activity and Stability for CO Oxidation. *Nanoscale* **2019**, *11* (14), 6776−6783.
(33) Gu, D.; Zheng, H.; Ma, Y.; Xu, S.; Zhou, X. A Highly-Efficient Approach for Reducing Phase Transition Temperature of VO_2 Polycrystalline Thin Films through Ru4+-Doping. *J. Alloys Compd.* **2019**, *790*, 602−609.
(34) Kunkalekar, R. K.; Salker, A. V. Activity of Pd Doped and Supported Mn_2O_3 Nanomaterials for CO Oxidation. *React. Kinet. Mech. Catal.* **2012**, *106* (2), 395−405.
(35) Zhou, Y.; Wang, Z.; Liu, C. Perspective on CO Oxidation over Pd-Based Catalysts. *Catal. Sci. Technol.* **2015**, *5* (1), 69−81.
(36) Abujarada, S.; Walton, A. S.; Thomas, A. G.; Chohan, U. K.; Koehler, S. P. K. Adsorption Site, Orientation and Alignment of NO Adsorbed on Au(100) Using 3D-Velocity Map Imaging, X-Ray Photoelectron Spectroscopy and Density Functional Theory. *Phys. Chem. Chem. Phys.* **2019**, *21* (21), 10939−10946.
(37) Szanyi, J.; Kwak, J. H. Dissecting the Steps of CO_2 Reduction: 1. The Interaction of CO and CO_2 with γ-Al_2O_3: An in Situ FTIR Study. *Phys. Chem. Chem. Phys.* **2014**, *16* (29), 15117−15125.
(38) López, J. M.; Gilbank, A. L.; García, T.; Solsona, B.; Agouram, S.; Torrente-Murciano, L. The Prevalence of Surface Oxygen Vacancies over the Mobility of Bulk Oxygen in Nanostructured Ceria for the Total Toluene Oxidation. *Appl. Catal., B* **2015**, *174*−*175*, 403−412.
(39) Qin, X.; Chen, M.; Chen, X.; Zhang, J.; Wang, X.; Fang, J.; Zhang, C. Effects of the Metal−Support Interaction in Ru/CeO_2 Nanostructures on Active Oxygen Species for HCHO/CO Oxidation. *ACS Appl. Nano Mater.* **2022**, *5* (10), 15574−15582.
(40) Sabaté, F.; Jordá, J. L.; Sabater, M. J.; Corma, A. Synthesis of Isomorphically Substituted Ru Manganese Molecular Sieves and Their Catalytic Properties for Selective Alcohol Oxidation. *J. Mater. Chem. A* **2020**, *8* (7), 3771−3784.
(41) Yao, X.; Tang, C.; Ji, Z.; Dai, Y.; Cao, Y.; Gao, F.; Dong, L.; Chen, Y. Investigation of the Physicochemical Properties and Catalytic Activities of $Ce_{0.67}M_{0.33}O_2$ (M = Zr^{4+}, Ti^{4+}, Sn^{4+}) Solid Solutions for NO Removal by CO. *Catal. Sci. Technol.* **2013**, *3* (3), 688−698.
(42) Khivantsev, K.; Jaegers, N. R.; Aleksandrov, H. A.; Song, I.; Pereira-Hernandez, X. I.; Engelhard, M. H.; Tian, J.; Chen, L.; Motta Meira, D.; Kovarik, L.; Vayssilov, G. N.; Wang, Y.; Szanyi, J. Single Ru(II) Ions on Ceria as a Highly Active Catalyst for Abatement of NO. *J. Am. Chem. Soc.* **2023**, *145* (9), 5029−5040.
(43) Roy, S.; Marimuthu, A.; Hegde, M. S.; Madras, G. High Rates of CO and Hydrocarbon Oxidation and NO Reduction by CO over $Ti_{0.99}Pd_{0.01}O_{1.99}$. *Appl. Catal., B* **2007**, *73* (3), 300−310.
(44) Díaz, J.; Buendía, G. M. A Model for the Catalytic Reduction of NO with CO and N Desorption. *Physica A* **2018**, *491*, 13−27.

https://doi.org/10.1021/acs.langmuir.4c01544
Langmuir 2024, 40, 15721−15730

(45) Li, J.; Ke, R.; Li, W.; Hao, J. Mechanism of Selective Catalytic Reduction of NO over Ag/Al_2O_3 with the Aid of Non-Thermal Plasma. *Catal. Today* **2008**, *139* (1−2), 49−58.
(46) Carlotto, S.; Natile, M. M.; Glisenti, A.; Vittadini, A. Catalytic Mechanisms of NO Reduction in a CO-NO Atmosphere at Co- and Cu-Doped $SrTiO_3$(100) Surfaces. *J. Phys. Chem. C* **2018**, *122* (1), 449−454.
(47) Gao, G.; Shi, J. W.; Fan, Z.; Gao, C.; Niu, C. MnM_2O_4 Microspheres (M = Co, Cu, Ni) for Selective Catalytic Reduction of NO with NH_3: Comparative Study on Catalytic Activity and Reaction Mechanism via in-Situ Diffuse Reflectance Infrared Fourier Transform Spectroscopy. *Chem. Eng. J.* **2017**, *325*, 91−100.
(48) Kim, H. Y.; Lee, H. M.; Henkelman, G. CO Oxidation Mechanism on CeO_2 -Supported Au Nanoparticles. *J. Am. Chem. Soc.* **2012**, *134* (3), 1560−1570.
(49) Sedmak, G.; Hočevar, S.; Levec, J. Kinetics of Selective CO Oxidation in Excess of H_2 over the Nanostructured $Cu_{0.1}Ce_{0.9}O_{2-Y}$ Catalyst. *J. Catal.* **2003**, *213* (2), 135−150.
(50) Okal, J.; Zawadzki, M.; Kraszkiewicz, P.; Adamska, K. Ru/CeO_2 Catalysts for Combustion of Mixture of Light Hydrocarbons: Effect of Preparation Method and Metal Salt Precursors. *Appl. Catal., A* **2018**, *549*, 161−169.
(51) Bera, P.; Patil, K. C.; Jayaram, V.; Hegde, M. S.; Subbanna, G. N. Combustion Synthesis of Nanometal Particles Supported on a-Al_2O_3: CO Oxidation and NO Reduction Catalysts. *J. Mater. Chem.* **1999**, *9*, 1801−1805.

https://doi.org/10.1021/acs.langmuir.4c01544
Langmuir 2024, 40, 15721−15730